




Cite this: DOI: 10.1039/d5sc03379a

All publication charges for this article have been paid for by the Royal Society of Chemistry

Photosensitized diradical rearrangement of alkenyl oxime ethers towards amino-featured oxiranes: reaction, mechanism, and structural prediction†

Tu-Ming Liu, Lin-Yuan Zhu, Min-Hao Qi, Si-Jia Li, Xiao-Jian Wang, Jia-Rui Xu and Bing Han *

A novel diradical rearrangement protocol of alkenyl ketoxime ethers for the synthesis of amino-featured epoxides under energy-transfer photocatalysis was developed. Mechanism studies revealed that this reaction was triggered by a specific diradical afforded by the second triplet excitation state T₂ resulting from the π - π^* excited transition of the alkene moiety of the substrate, followed by a cascade radical remote amino group translocation and intramolecular singlet O-, C-diradical cross-coupling after intersystem crossing. As a result, a series of amino-featured epoxides that were previously inaccessible, were synthesized easily and efficiently. Notably, this approach featured mild conditions, good functional group tolerance, excellent stereoselectivity and was very compatible with complex scaffolds (steroids, amino acids, alkaloids). Detailed density functional theory (DFT) calculations provided in-depth insights into the understanding of the reaction as well as structural standards and predictions. This strategy not only enriches the reaction mode of the oxime ethers but also provides a facile synthetic method towards valuable epoxides.

Received 9th May 2025
Accepted 30th June 2025

DOI: 10.1039/d5sc03379a
rsc.li/chemical-science

Introduction

As a three-membered oxa-heterocycle with a unique structure, oxirane is found widely in natural products and drug molecules¹ (Scheme 1A). In addition, due to its high ring tension and strongly polarized C–O bond, oxirane also serves as a key synthon in organic synthesis by affording various functional group transformations.^{2,3} Therefore, the efficient and convenient construction of the oxirane structure has been an important focus of organic synthesis. Many strategies have been developed for this purpose: intramolecular nucleophilic substitution of alcohols with a leaving group at the β -position;⁴ epoxidation of alkenes;⁵ Corey–Chaykovsky epoxidation of aldehydes and ketones;⁶ Payne rearrangement⁷ (Scheme 1B). Despite great achievements, existing methods face several limitations, including poor compatibility with highly active functional groups, unsatisfactory suppression of side reactions caused by the oxidative sensitivity of the substrate, as well as the poor chemo-/site-selectivity of the substrates with multiple olefins and carbonyls. Especially for an amino-containing oxirane, which act as units with specific toxicity against cancer cells,^{1f,g}

conventional tactics face problems of inefficiency and product complexity due to the nucleophilicity and oxidative sensitivity of the amine group.⁸ Thus, the development of novel strategies for the efficient access to oxirane, especially for the amino-containing counterpart, is of great significance and value for the chemistry of organic and medicinal compounds.

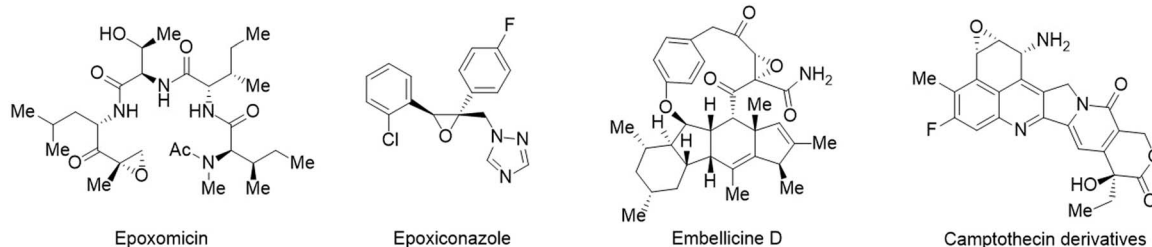
Oximes, as a class of fundamental organic compounds, have been widely used in diverse organic transformations, including traditional ionic conversions and emerging radical reactions. The former are known for the Beckmann rearrangement,⁹ reductive amination,¹⁰ and transition metal-catalysed cross-coupling,¹¹ whereas the latter are represented by iminoxyl radical-mediated O/N-atom dichotomous cyclization¹² and iminyl radical-mediated diverse reactions.¹³ In recent years, visible light-mediated photocatalytic energy transfer (EnT) has provided an opportunity to develop sustainable chemical conversions using triplet-state diradicals.¹⁴ Accordingly, some oxime-mediated novel transformations have been undertaken with the help of the EnT tactic.^{15–17} For example, a series of olefin difunctionalizations has been reported by Glorius and colleagues¹⁶ and other research teams (including ours¹⁷) independently. In addition, some elegant intra-/intermolecular [2 + 2] cycloadditions of oximes with olefins have been reported by Schindler *et al.*¹⁸ Based on our continuing interest in the research of oximes conversion,¹⁹ we wondered if it is possible to use oximes for synthesizing amino group-containing epoxides by taking advantage of their natural structural features.

State Key Laboratory of Natural Product Chemistry, College of Chemistry and Chemical Engineering, Lanzhou University, Lanzhou, 730000, China. E-mail: hanb@lzu.edu.cn

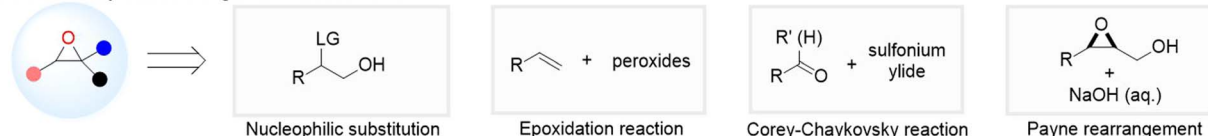
† Electronic supplementary information (ESI) available. CCDC 2439472. For ESI and crystallographic data in CIF or other electronic format see DOI: <https://doi.org/10.1039/d5sc03379a>



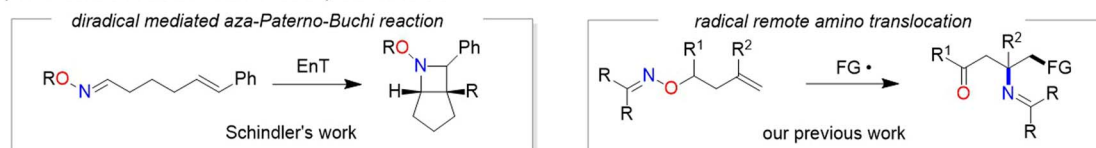
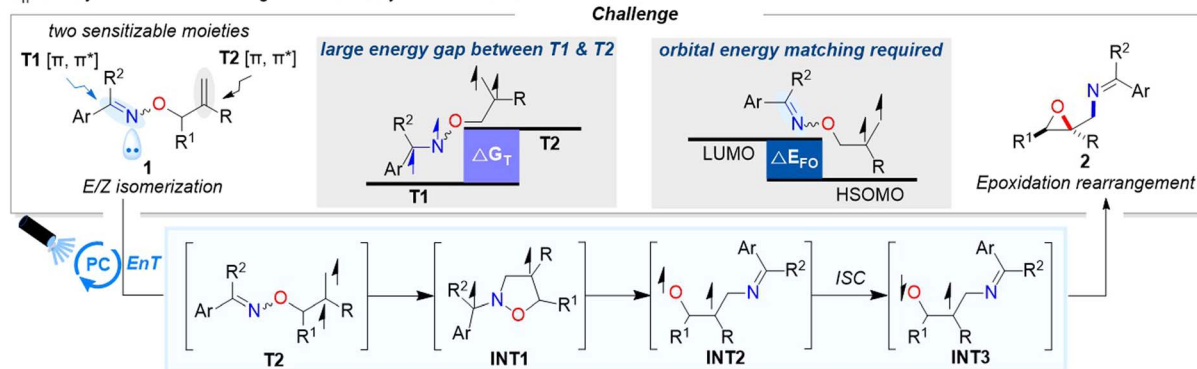
A Natural products and drugs containing oxiranes



B Available synthetic strategies to access oxiranes



C Representative conversion modes of alkenyl oxime ethers

D E_nT -catalyzed diradical rearrangement of alkenyl oximes to access oxiranes

Scheme 1 Synthetic strategy for oxiranes and the representative mode of the alkenyl oxime reaction.

We were encouraged by our recent work on the radical remote amino translocation of alkenyl oximes by N–O bond cleavage (Scheme 1C).²⁰ Hence, we anticipated that this translocation may also be applicable to a triplet-state diradical counterpart.²¹ We speculated that if the alkenyl moiety of oxime **1** is excited to its triplet-state T_2 through EnT-mediated photocatalysis, the fast 5-*exo-trig* cyclization of the terminal C-radical to the imine moiety would lead to the formation of a five-membered triplet diradical intermediate **INT1**. By employing the radical β -scission of a weak N–O bond, a triplet O-, N-diradical intermediate **INT2** would be formed, which subsequently undergoes intersystem crossing (ISC) to generate singlet diradical counterpart **INT3**. Finally, the desired amino-contained oxiranes **2** would be realized *via* intramolecular cross-coupling between the O-radical and C-radical (Scheme 1D). However, due to the coexistence of imine and alkene moieties in oxime **1**, the hypothesized epoxidation reaction faces three challenges: (1) energy transfer sensitization competition between the C=N bond and C=C bond with the excited photocatalyst; (2) the supposed reaction begins from the

high-energy-level T_2 by sensitization of the alkene moiety rather than the low-energy-level T_1 by sensitization of the imine moiety, which leads to the deactivation of T_2 by an internal conversion to T_1 ; (3) T_1 and T_2 are inclined to undergo the alternative relaxation, including non-radiation *Z-E* isomerization of alkenyl oxime **1** and radiative deexcitation.

To overcome the above-mentioned challenges, we assumed that two factors would facilitate the desired reaction: (1) introducing styrene or the conjugated diene into oxime **1** and using a photocatalyst with high E_T to ensure the efficient sensitization of the olefin moiety; (2) increasing the Gibbs free energy gap ($\Delta G_T = G_{T_2} - G_{T_1}$) between T_2 and T_1 states to avoid the inactivation of the T_2 state by internal conversion; (3) reducing the energy gap ($\Delta E_{FO} = E_{LUMO[\text{oxime}]} - E_{HSOMO[\text{alkene}]}$) between the highest singly occupied molecular orbital (HSOMO) of the alkenyl diradical and the lowest unoccupied molecular orbital (LUMO) of the C=N bond to increase the frontier orbital matching ability of the cyclization process, thereby suppressing the unwanted alternative relaxation. By employing the aforementioned strategy, the desired oxiranes **2** were produced by



the photocatalytic epoxidation rearrangement of the readily available alkenyl oximes. This reaction provides a new method for synthesizing amino oxiranes that were previously inaccessible and broadens the boundary of the reaction mode of oximes.

Results and discussion

The present study commenced with the irradiation of a mixture of styrene-tethered oximes **1** and organic photosensitizer 2,4,5,6-tetra(9*H*-carbazol-9-yl) isophthalonitrile (4CzIPN) in ethyl acetate with blue light (443 nm, 30 W). First, the reaction optimization was carried out with aldoximes. However, benzaldehydoxime **E-1-A** underwent only *Z/E*-isomerization to give a mixture of **1-A** with a ratio of *Z:E* of 8:1, and the desired oxirane **2-A** was not detected. Similarly, benzaldehydoximes **E-1-B** and **E-1-C** bearing an electron-donating methoxy group and electron-withdrawing trifluoromethyl group on the *para*-position of phenyl ring, respectively, only underwent *Z/E*-isomerization as well (Table 1,

entries 2 and 3). In addition, methyl glyoxylatoxime **E-1-D** was inert under the reaction conditions, and no reaction (even *Z-E* isomerization) occurred (Table 1, entry 4). Apparently, the aldoxime structure was not suitable for the protocol. Subsequently, we explored the reactivity of ketoximes by varying structural features under these conditions. Neither acetophenoxime **E-1-E** nor acetoxime **1-F** could be converted into the desired products. The former underwent only *Z-E* isomerization, whereas the latter was inert in the reaction (Table 1, entries 5 and 6). Delightedly, diphenylketoxime **1a** succeeded in obtaining the desired oxirane **2a** in 82% yield (Table 1, entry 7). Next, other photocatalysts, such as thioxanthone (TXT), *fac*-Ir(ppy)₃ (Ir), and [Ir(dF(CF₃)ppy)₂(dtbbpy)]PF₆ (Ir-F) with different triplet-state energy (*E*_T), were also tested in the reaction. Although they could also afford **2a**, its yield failed to improve, presumably due to inadequate photosensitization under blue light or lower triplet-state energy (Table 1, entries 8–10). Unfortunately, when Ru(bpy)₃(PF₆)₂ [Ru] acted as the photocatalyst, no reaction occurred and **1a** was fully recovered, possibly due to its EnT

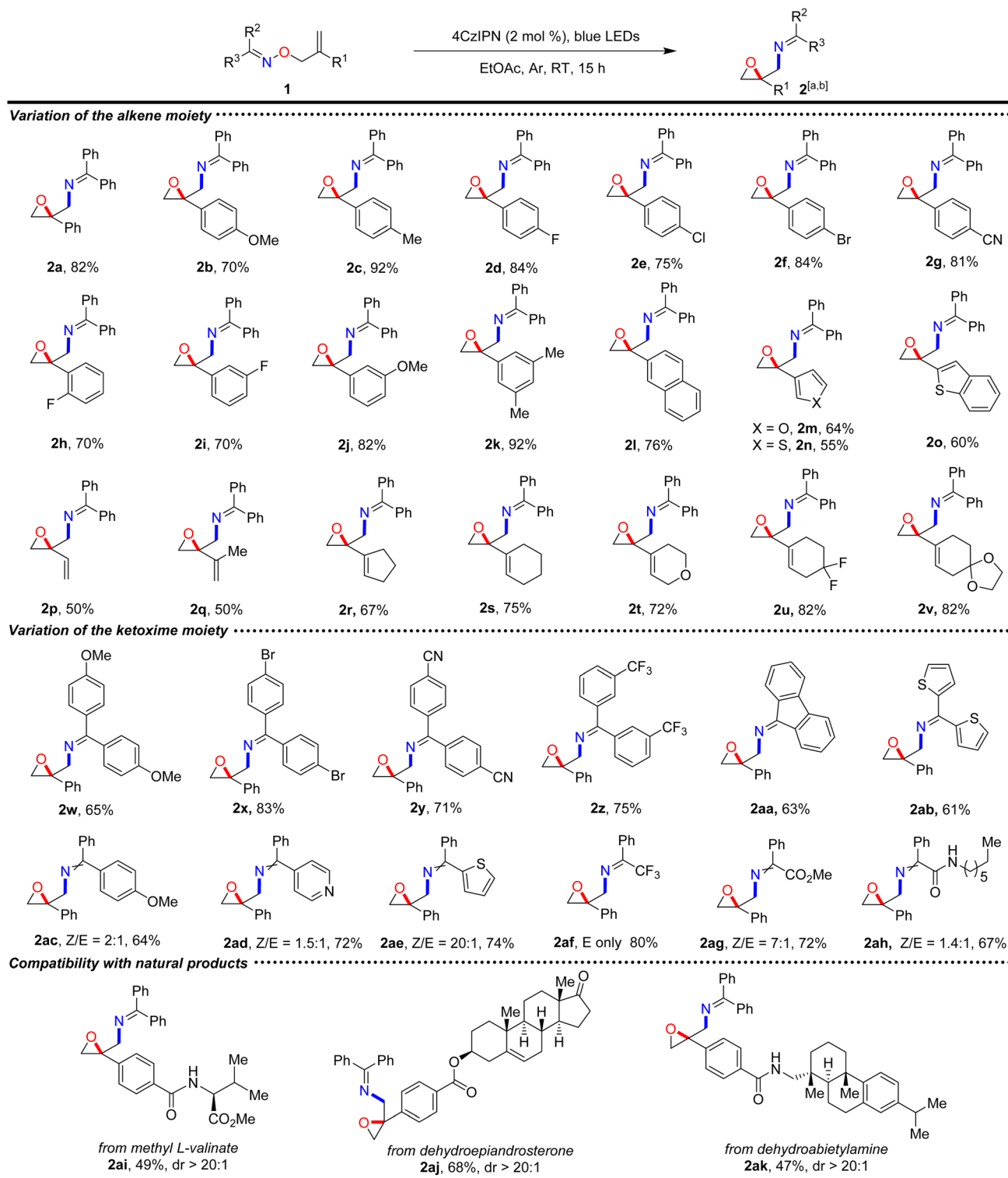
Table 1 Optimization of the oxime structure and reaction conditions^a

<p>Ru(bpy)₃(PF₆)₂ [Ru] <i>E</i>_T: 46.0 kcal/mol <i>E</i>_{1/2}^{[M^{•+}]/[M^{•+}]}: +0.77 V <i>E</i>_{1/2}^{[M^{•+}]/[M^{•+}]}: -0.81 V</p> <p><i>fac</i>-Ir(ppy)₃ [Ir] <i>E</i>_T: 58.1 kcal/mol <i>E</i>_{1/2}^{[M^{•+}]/[M^{•+}]}: +0.31 V <i>E</i>_{1/2}^{[M^{•+}]/[M^{•+}]}: -1.73 V</p> <p>2,4,5,6-tetra(9<i>H</i>-carbazol-9-yl) isophthalonitrile [4CzIPN] <i>E</i>_T: 61.6 kcal/mol <i>E</i>_{1/2}^{[M^{•+}]/[M^{•+}]}: +1.43 V <i>E</i>_{1/2}^{[M^{•+}]/[M^{•+}]}: -1.18 V</p> <p>[Ir(dF(CF₃)ppy)₂(dtbbpy)]PF₆ [Ir-F] <i>E</i>_T: 61.8 kcal/mol <i>E</i>_{1/2}^{[M^{•+}]/[M^{•+}]}: +1.21 V <i>E</i>_{1/2}^{[M^{•+}]/[M^{•+}]}: -0.89 V</p> <p>thioxanthone [TXT] <i>E</i>_T: 65.5 kcal/mol <i>E</i>_{1/2}^{[M^{•+}]/[M^{•+}]}: +1.18 V <i>E</i>_{1/2}^{[M^{•+}]/[M^{•+}]}: -1.11 V</p>							
EnT →							
Entry	Substrate			Photocatalyst	Solvent	Yield ^{a,b} (%)	
	R ¹	R ²	<i>Z/E</i>			1 (% <i>Z/E</i>)	2
1	Ph	H	1A , 0/1	4CzIPN	EtOAc	1A , 80, 8/1	2A , 0
2	<i>p</i> -MeOPh	H	1B , 0/1	4CzIPN	EtOAc	1B , 85, 6/1	2B , 0
3	<i>p</i> -CF ₃ Ph	H	1C , 0/1	4CzIPN	EtOAc	1C , 88, 5/1	2C , 0
4	CO ₂ Me	H	1D , 0/1	4CzIPN	EtOAc	1D , 98%, 0/1 ^c	2D , 0
5	Ph	Me	1E , 0/1	4CzIPN	EtOAc	1E , 88, 5/1	2E , 0
6	Me	Me	1F , —	4CzIPN	EtOAc	1F , —	2F , 0
7	Ph	Ph	1a , —	4CzIPN	EtOAc	0	2a , 82
8	Ph	Ph	1a , —	TXT	EtOAc	0	2a , 42
9	Ph	Ph	1a , —	Ir-F	EtOAc	0	2a , 78
10	Ph	Ph	1a , —	[Ir]	EtOAc	0	2a , 70
11	Ph	Ph	1a , —	[Ru]	EtOAc	1d , 98, — ^c	2a , 0
12	Ph	Ph	1a , —	4CzIPN	MeCN	0	2a , 63
13	Ph	Ph	1a , —	4CzIPN	MeOH	0	2a , 60
14	Ph	Ph	1a , —	4CzIPN	DCM	0	2a , 0
15	Ph	Ph	1a , —	—	EtOAc	95, — ^c	2a , 0
16	Ph	Ph	1a , —	4CzIPN	EtOAc	80, — ^{c,d}	2a , 0

^a Reaction conditions: 0.2 mmol scale, PC (2 mol%), solvent (0.1 M), 30 W 443 nm blue LEDs, 15 h. ^b Isolated yields. ^c No reaction occurred, and the starting material was recovered. ^d Reaction was conducted in the dark.

being too low to sensitize **1a** effectively (Table 1, entry 11). In addition, solvent screening showed that ethyl acetate was the best one (Table 1, entries 12–14). Both the photocatalyst and light irradiation were indispensable for an efficient reaction to proceed, clearly supporting a photocatalytic mechanism (Table 1, entries 15 and 16).

To evaluate the applicability of the protocol, various alkenyl ketoxime ethers were investigated under the optimal reaction conditions, as shown in Scheme 2. The scope of the alkene moiety was first explored. Styrene moieties with substituents of different electronic properties on the *para*-position of the phenyl ring, such as OMe, Me, F, Cl, Br, CN, were all compatible



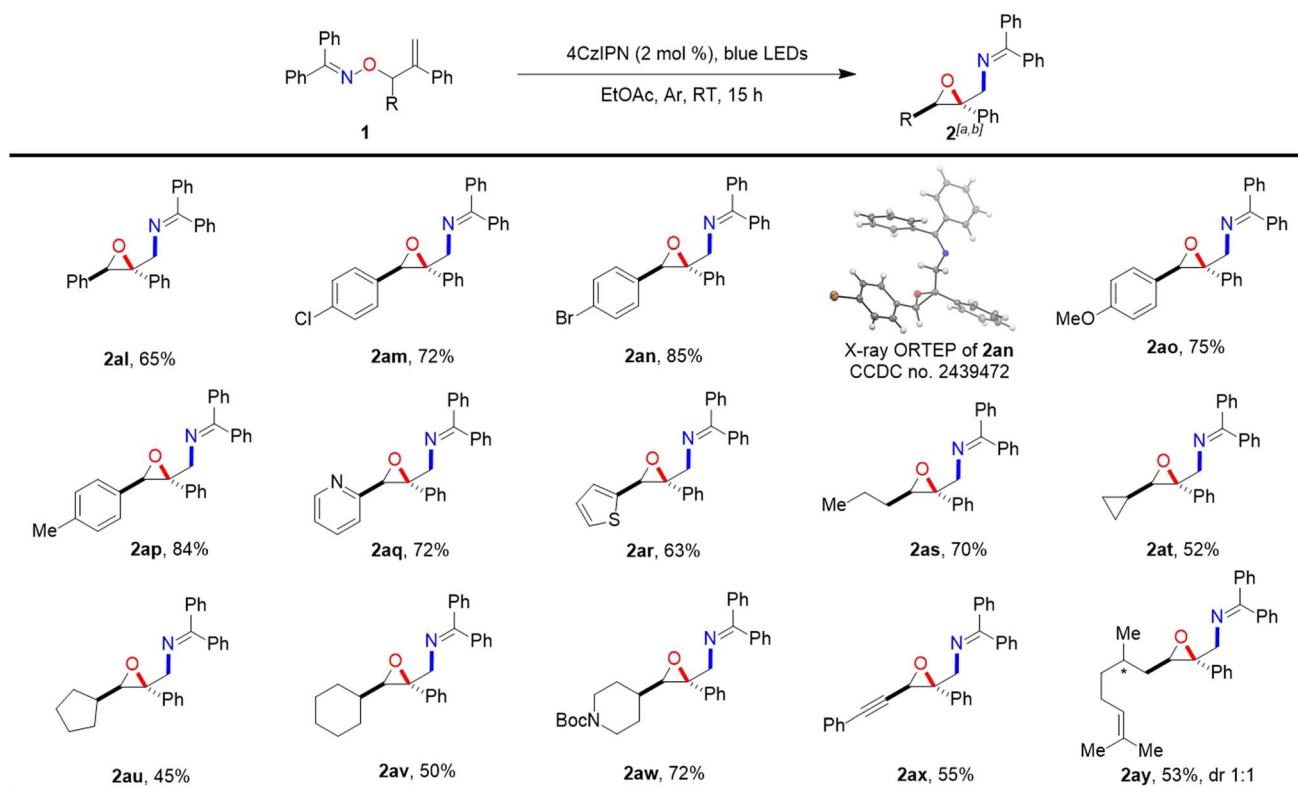
Scheme 2 ^aReaction conditions: 0.2 mmol scale, 4CzIPN (2 mol%), EtOAc (0.1 M), blue LEDs (443 nm, 30 W), 15 h. ^bIsolated yields.



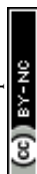
with the reaction conditions, and converted smoothly to the corresponding amino-tethered oxiranes **2b–2g** in good (70%) to excellent (92%) yields. Accordingly, *ortho*-/ *meta*-fluoro and *meta*-methoxy substituted styrenes also reacted very well using this approach, delivering the desired products **2h–2j** in good yields. Dimethyl-substituted styrene was also suitable for the reaction, affording the desired product **2k** in 92% yield. Both electron-rich and electron-deficient styrenes could be converted in the reaction, indicating that electronic effects did not influence the reaction. In addition to styrenes, other aryl and heteroaryl groups incorporated into ethenes, such as naphthyl, furan, thiophene, and benzothiophene, were all good partners for the reaction, as demonstrated in cases **2l–2o**, in which the corresponding oxiranes were formed in moderate (55%) to good (76%) yields. Importantly, the protocol could be extended readily from aryl-substituted alkenes to 1,3-dienes, establishing a novel approach for the regioselective functionalization of conjugated dienes. Acyclic and cyclic conjugated 1,3-dienes were good candidates for this method. Acyclic 1,3-dienes, such as 1,3-butadiene and isoprene, were efficiently transformed in the reaction, yielding products **2p** and **2q** in 50% yields. Cyclic dienes, such as cyclopentene- and cyclohexene-fused ethenes, proceeded smoothly and provided products **2r** and **2s** in 67% and 75% yields, respectively. O-atom-embedded and difluoro-substituted cyclohexenes converted smoothly as well, resulting in the corresponding products **2t–2u** in excellent yields. When the ketal-containing cyclohexene was employed in the conversion, the desired product **2v** was obtained in 82% yield,

suggesting the potential for constructing epoxy-ketone architectures. Subsequently, the boundary of the oxime moiety was explored using the tethered styrene as the reaction partner. Symmetric diaryl ketoximes, represented by benzophenonoximes bearing *para*-methoxy, *para*-bromo, *para*-cyano, and *meta*-trifluoromethyl on the phenyl rings, were good candidates and converted to the corresponding products **2w–2z** in good yields, and no significant electronic effects were observed. Furthermore, 9-fluorenonoxime and thienylketoxime also showed good compatibility, giving products **2aa** and **2ab** in 63% and 61% yields, respectively. Notably, asymmetric diaryl ketoximes, such as *p*-MeO-phenyl-phenyl, phenyl-pyridinyl, and phenyl-thienyl ketoximes, were also very compatible with the protocol, as demonstrated in cases **2ac–2ae**. Delightfully, in addition to diaryl ketoximes, monoaryl ketoximes bearing electron-deficient groups, such as CF₃, ester, and amide, also performed very well under the conditions, affording the desired products **2af–2ah** in 67–80% yields. Importantly, this approach was also compatible with complex natural scaffolds, such as amino acids, steroids, and alkaloids, as in cases **2ai–2ak**, showing a promising application for late-stage modification.

Having achieved 1,1-disubstituted oxiranes by this method, we hope that it was also suitable for synthesizing the 1,1,2-trisubstituted counterparts using secondary alkenyl alcohol-derived benzophenonoximes ethers as substrates. To our delight, the protocol was suitable for obtaining 1,1,2-trisubstituted oxiranes and exhibited a single diastereoselectivity for 1,2-substitutions, and the results are summarized in Scheme 3.



Scheme 3 ^aReaction conditions: 0.2 mmol scale, 4CzIPN (2 mol %), EtOAc (0.1 M), blue LEDs (443 nm, 30 W), 15 h. ^bIsolated yields.

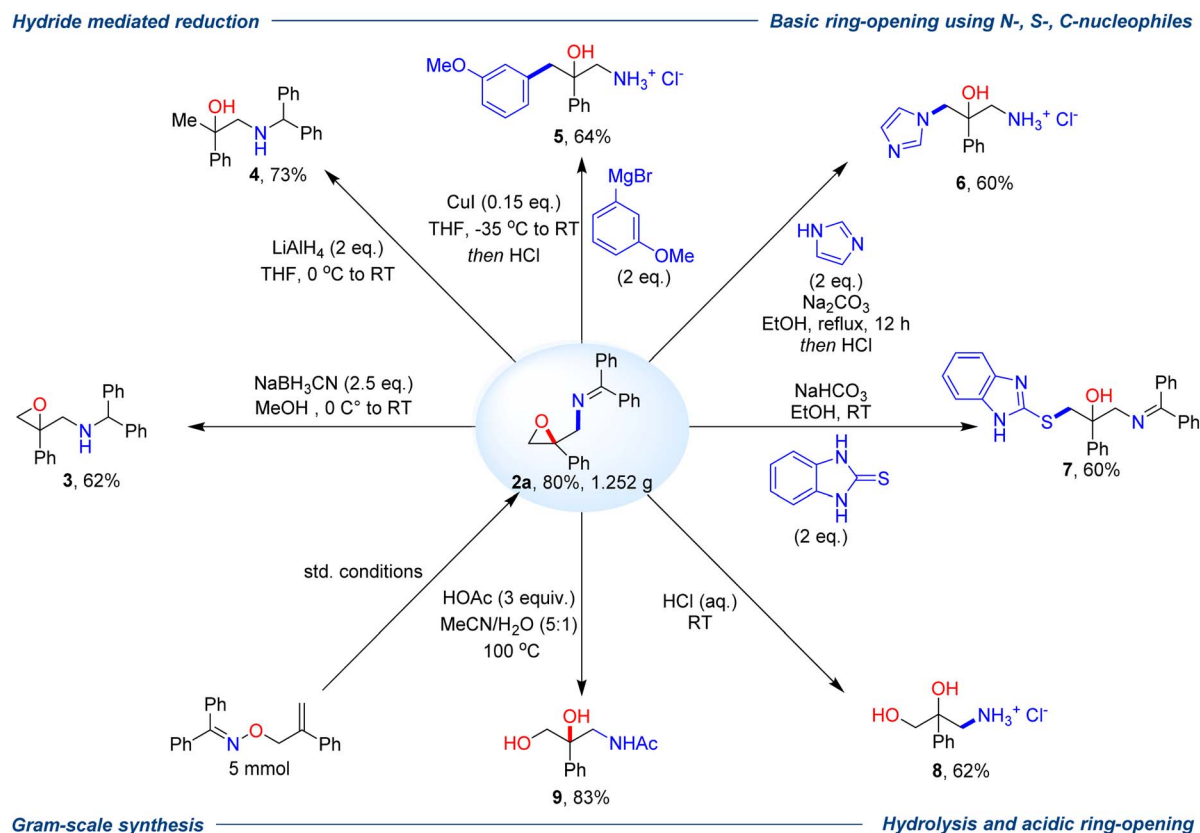


Ketoxime ethers bearing a series of substituted phenyls with different electronic properties at the α -position of the O-atom reacted very well in the reaction and produced the corresponding products **2al–2ap** in good yields as single diastereomers. The structure and configuration of epoxide **2an** were confirmed by X-ray crystallography.²¹ When the aforementioned phenyls were replaced by pyridinyl and thienyl, the conversions were smooth, giving rise to **2aq** and **2ar** in 72% and 63% yields, respectively. Notably, the substitution of phenyl by alkyl chains or cycloalkyls did not affect the reactivity, as demonstrated in cases **2as–2aw**, in which propyl, cyclopropyl, cyclopentyl, cyclohexyl, and piperidinyl were involved. In particular, ketoxime ethers that replaced the phenyl group with alkynyl and alkenyl groups were also converted to the desired products **2ax** and **2ay** in yields of 55% and 53%, respectively.

To further prove the practicability and suitability of our protocol, the gram-scale synthesis and diverse derivation of the amino group-containing oxiranes were carried out, as shown in Scheme 4. The gram-scale synthesis was performed at a 5 mmol scale using substrate **1a**, producing oxirane **2a** at 1.252 g in 80% yield. Further conversions of **2a** were conducted by various transformations of functional groups, such as reduction, hydrolysis, and epoxy ring-opening. The reduction of **2a** could be smoothly achieved using NaBH_3CN and LiAlH_4 , respectively. The former provided the diphenylamine oxirane **3** in 62% yield by solely reducing the imine moiety, and the latter produced 2-amino tertiary alcohol **4** in 73% yield by simultaneously

reducing imine and epoxy moieties. Using C-, N- and S-nucleophiles, such as phenyl Grignard reagent, imidazole, and 2-mercaptobenzimidazole to react with **2a**, tertiary alcohols **5–7** were generated in good yields by the nucleophilic epoxy ring-opening concomitant with the forging of C–C, N–C, and S–C bonds, respectively. Importantly, when **2a** was treated with muriatic acid, the hydrolysis of the imine and acidic ring-opening was also achieved, affording the structurally valuable 3-amino-2-phenylpropane-1,2-diol hydrochloride **8** in 62% yield. Acetamide-incorporated 1,2-diol **9** was obtained in 83% yield by a cascade hydrolysis, acylation, and acidic epoxy ring-opening after being treated with acetic acid under heating.

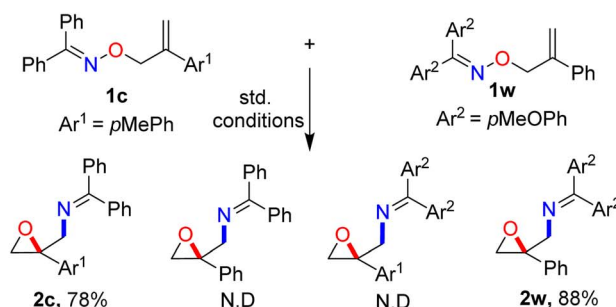
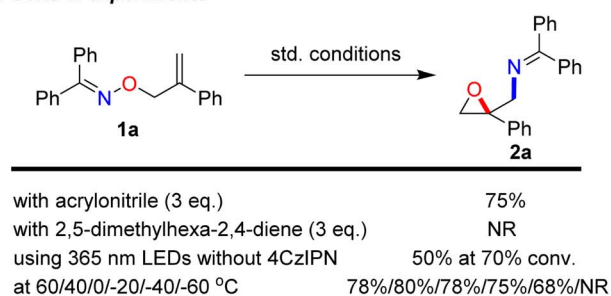
To understand the reaction mechanism of this protocol, control experiments, cyclic voltammetry, UV-visible absorption, and Stern–Volmer experiments were carried out, as shown in Scheme 5. When the triplet reaction inhibitor 2,5-dimethylhexa-2,4-diene was added, the desired reaction was completely inhibited in the sample reaction. In contrast, the reaction proceeded smoothly, and the product **2a** was obtained in 75% yield when the singlet reaction inhibitor acrylonitrile was added. In addition, the sample reaction still occurred under the direct-irradiation with violet LEDs (365 nm, 20 W) in the absence of a photocatalyst, despite delivering **2a** in 50% yield under a conversion rate of 70%. These results indicated that the protocol experienced a triplet photoreaction by energy-transfer catalysis. The influence of temperature on the reaction was also investigated. The reaction could proceed effectively between



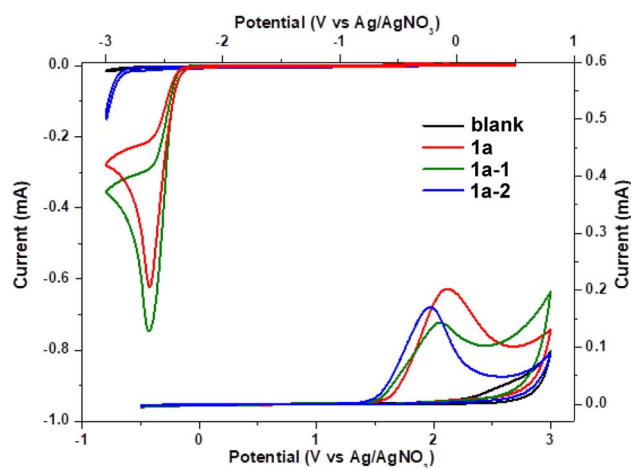
Scheme 4 Gram-scale synthesis and derivatization of oxiranes.



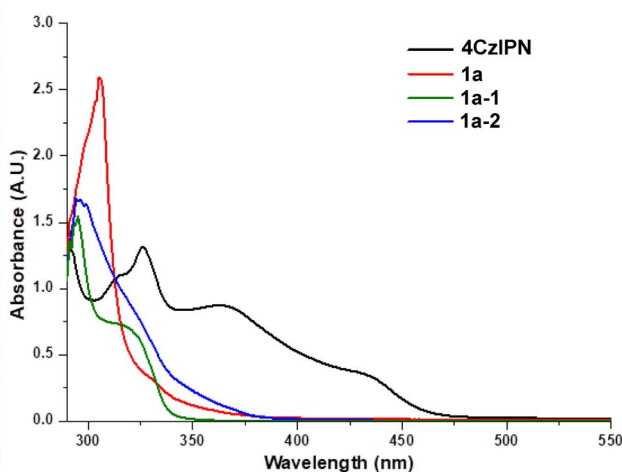
A) Control experiments



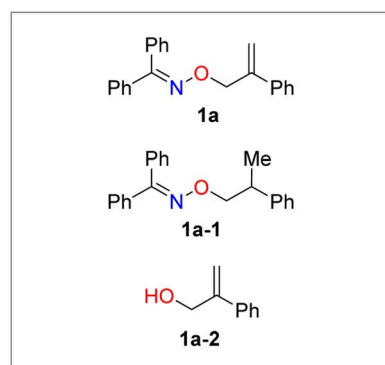
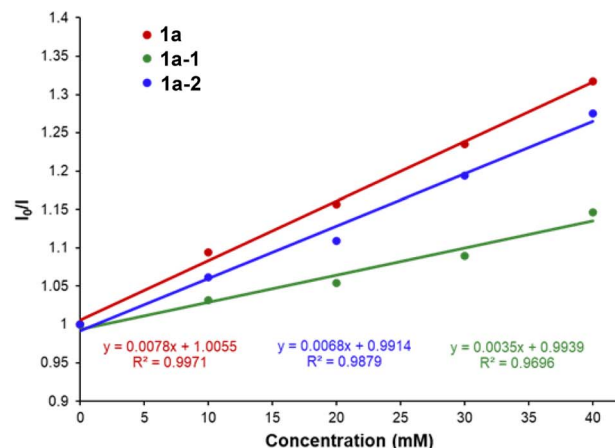
B) Cyclic voltammetry



C) UV-Vis absorption



D) Stern-Volmer quenching experiments



Scheme 5 Mechanism studies.

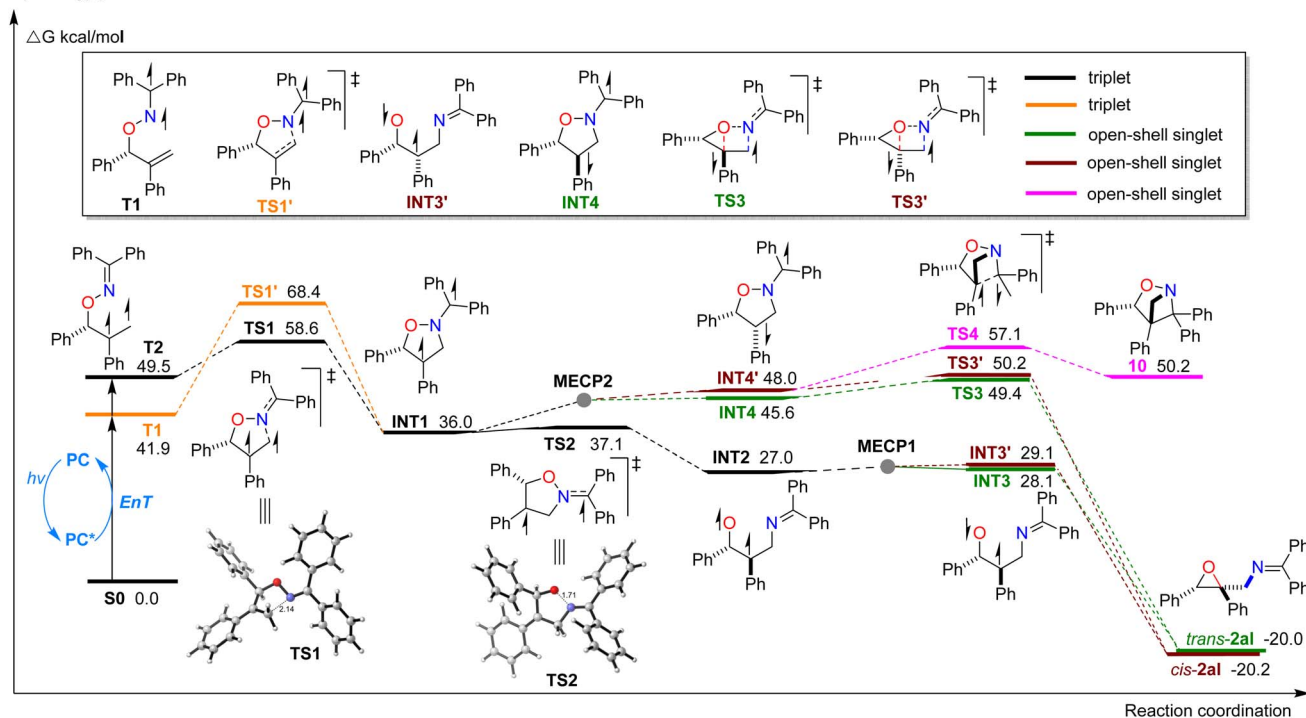
−40 °C and +60 °C, and the yield of **2a** was almost unaffected. However, the reaction was completely inhibited at −60 °C, probably because sufficient activation energy could not be provided for the reaction at such a low temperature. Moreover, crossover experiments demonstrated that under standard reaction conditions, the concurrent addition of substrates **1c** and **1w** afforded epoxides **2c** (78% yield) and **2w** (88% yield) exclusively, with no detectable formation of other epoxides. These results indicated that the reaction experienced an intramolecular cleavage and recombination of the N–O bond. UV-Vis absorption

spectra clearly showed that ketoxime **1a** did not have obvious absorption above 400 nm, and weak absorption at 350 nm. These data indicated that it could not be excited by blue light, but could be excited by UV light, which was completely consistent with our experimental results. The measured oxidation potential E_{ox} of ketoxime **1a** was 2.1 V, while its reduction potential E_{red} was lower than −2.0 V, implying that the effective REDOX reaction could not occur between **1a** and the excited photocatalyst 4CzIPN and was more likely to follow an energy-transfer process. Moreover, Stern–Volmer quenching experiments clearly showed that

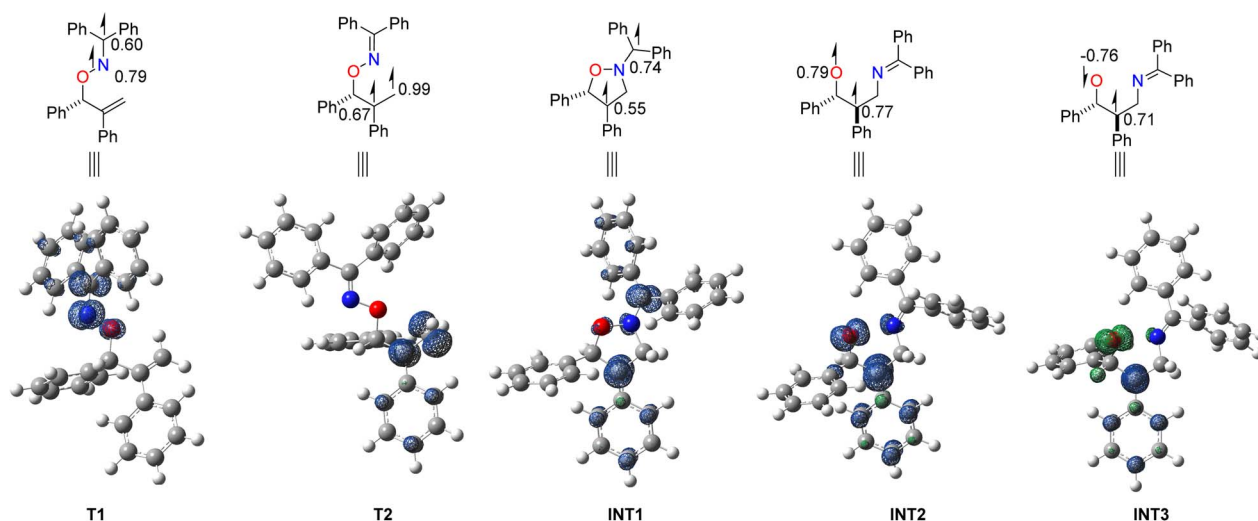
ketoimine **1a** could be quenched by the excited 4CzIPN. Compound **1a** had the C=N double bond of the oxime moiety and the C=C double bond of olefin moiety that could both be sensitized by a photosensitizer to trigger the reaction. Hence, we tried to determine which site of the reaction was triggered. Thus, compounds **1a-1** and **1a-2** as analogues of **1a** were also investigated under Stern–Volmer quenching experiments. Apparently, both the alkene moiety and oxime moiety could be quenched by the excited 4CzIPN.

To further confirm the initiation site and the mechanism of this diradical rearrangement reaction as well as to account for the excellent diastereoselectivity, density functional theory (DFT) calculations were conducted using **1a** as the model. The calculated energy profiles are illustrated in Scheme 6A. The obtained **T1** triplet state with an energy of 41.9 kcal mol^{−1} was caused by sensitization of the C=N bond, whereas the **T2** triplet state with an energy of 49.5 kcal mol^{−1} was caused by sensitization of the C=C bond. Apparently, the iminyl moiety had lower

A) Energy profile of the reaction coordinate



B) Atomic spin population analysis and spin density visualization.



Scheme 6 (A) DFT-calculated energy profiles for the reaction and rationalization of the excellent diastereoselectivity of compound **2a**. (B) Analysis of the atomic spin population and spin density visualization (blue isosurfaces indicate regions of positive spin density, and green isosurfaces indicate regions of negative spin density, at an isovalue of 0.01 a. u.). All calculations were performed at the B3LYP/def2-TZVP, SMD(EA)/B3LYP/6-31G(d,p) level with Gaussian 16. Gibbs free energies are given in kcal mol^{−1}. For details, see the ESI.†



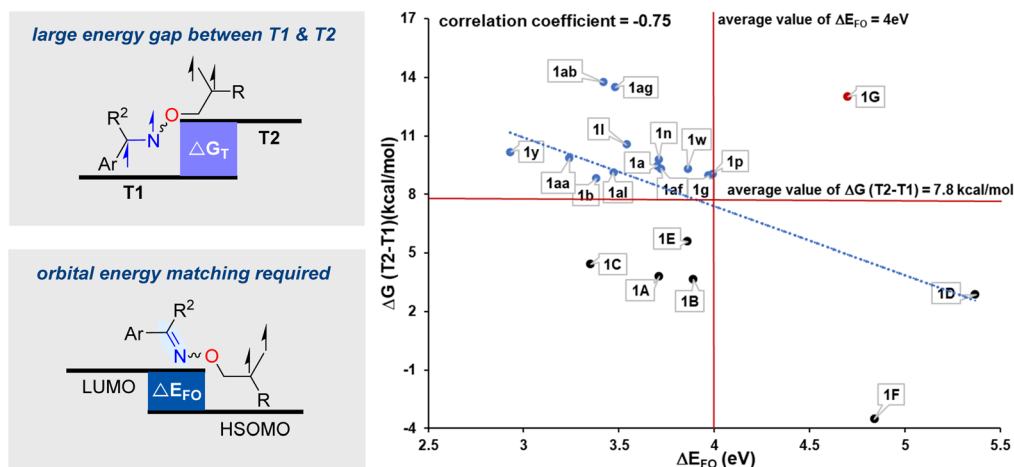
sensitization energy and was more easily sensitized than olefin. Theoretically, **T1** and **T2** states can form the same triplet diradical intermediate **INT1** by *N*-radical-mediated 5-*endo-trig* cyclization to olefin via **TS1'** ($\Delta G^\ddagger = 26.5 \text{ kcal mol}^{-1}$) and C-radical-mediated 5-*exo-trig* cyclization to oxime via **TS1** ($\Delta G^\ddagger = 9.1 \text{ kcal mol}^{-1}$), respectively. However, the activation energy of **TS1'** was much higher than that of **TS1** ($\Delta\Delta G^\ddagger = 17.4 \text{ kcal mol}^{-1}$), and therefore, it is more reasonable to initiate the reaction from the higher energy **T2** state despite the **T1** state being readily produced. This view was also consistent with the experimental result showing that the low-energy photosensitizer Ru(bpy)₃(PF₆)₂ ($E_T = 46.0 \text{ kcal mol}^{-1}$) failed to trigger the reaction. Next, we calculated two possible paths from **INT1** to product **2al**.

One was a stepwise path that experiences the β -scission of the O–N bond to produce the O-radical and subsequent intramolecular cross-coupling of the O-radical and C-radical to yield **2al**. The other was a concerted path in which cleavage of the N–O bond and formation of the C–O bond were carried out simultaneously without formation of the O-radical. In the first path, the calculated energy barrier for the cleavage of the O–N bond to produce the triplet diradical **INT2** through **TS2** was only $1.1 \text{ kcal mol}^{-1}$, indicating that formation of the O-radical was very easy due to the weak N–O bond, as we reported previously.²⁰ **INT2** could be transformed further into two configurations of singlet diradicals **INT3** and **INT3'** by ISC via the minimal energy crossing point (MECP). The intramolecular O- and C-radicals cross-coupling of the singlet diradicals **INT3** and **INT3'** finally produced the products *trans*-**2al** and *cis*-**2al**, respectively. This formation of the O–C bond by radical cross-coupling was

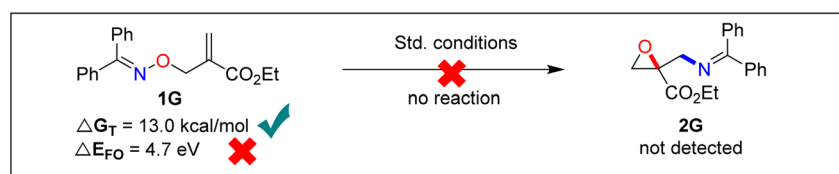
a barrierless process. Hence, the distribution of the products *trans*-**2al** and *cis*-**2al** could be determined by the energies of **INT3** and **INT3'** according to the Curtin–Hammett principle. Apparently, **INT3** had $1.0 \text{ kcal mol}^{-1}$ lower energy than **INT3'**, resulting in the formation of only *trans*-**2al** without *cis*-**2al**, which was consistent with the experimental observation. In the second path, **INT1** first underwent ISC via **MECP2** to produce singlet diradicals **INT4** and **INT4'**. The latter would also produce *cis*-**2al** and *trans*-**2al** via the bicyclic transition states **TS3'** ($\Delta G^\ddagger = 2.2 \text{ kcal mol}^{-1}$) and **TS3** ($\Delta G^\ddagger = 3.8 \text{ kcal mol}^{-1}$), respectively. However, the conversion of **INT4'** to product **10** in the form of cross-coupling of two C-radicals via **TS4** looked impossible because of a higher energy barrier of $9.1 \text{ kcal mol}^{-1}$ compared with that for the conversion of **INT4'** to *cis*-**2al** via **TS3'** with a lower activation energy. The concerted process provided an alternative path to access **2al**. However, considering that the ISC of this pathway requires more energy ($\Delta\Delta G = 9.6$ and $12.0 \text{ kcal mol}^{-1}$, respectively) and that the activation energies of **TS3** and **TS3'** are both higher than that of **TS2**, we believe that the stepwise path is more favorable than the concerted pathway.

Next, we tried to elucidate the features of alkenyl oximes **1** that enabled the epoxidation rearrangement to occur smoothly because aldoxime and some ketoximes did not undergo the reaction (as shown in the optimization). Initially, we thought that in addition to the efficient sensitization of alkenes, there were two important factors that would synergistically affect the epoxidation reaction. One factor was that the energy difference ($\Delta G_T = G_{T2} - G_{T1}$) of the excited triplet states **T1** and **T2** must be large enough to hinder the decay of **T2** by internal conversion, thus

A) Core criteria for the structural requirements of alkenyl oxime ethers



B) Prediction application



Scheme 7 Core criteria for the structural requirements of alkenyl oxime ethers in epoxidation rearrangement reactions and application of the structural prediction.



ensuring its smooth cyclization. The other factor was that matching the frontier orbital energy levels ($\Delta E_{\text{FO}} = E_{\text{LUMO}[\text{oxime}]} - E_{\text{HSOMO}[\text{alkene}]}$, serving as a measure of frontier orbital energy) of the alkene diradical and oxime would lead to a favorable 5-*exo-trig* cyclization by reducing the activation energy ΔG^\ddagger and ultimately promoting reactivity. To verify this hypothesis, we computed ΔG_{T} and ΔE_{FO} across a series of alkenyl oximes by DFT calculations, and the results are summarized in Scheme 7A by means of quadrant analyses. The reactive substrates were concentrated in the second quadrant of the diagram. That is, the reaction could proceed smoothly if the frontier orbitals were matched ($\Delta E_{\text{FO}} < 4$ eV) and the energy gap between **T1** and **T2** was large enough ($\Delta G_{\text{T}} > 7.8$ kcal mol⁻¹). However, the substrates that met only one of these two factors failed to achieve the desired conversion. For instance, alkenyl oximes **1A**, **1B**, **1C**, and **1E** that satisfied the former factor ($\Delta E_{\text{FO}} < 4$ eV) but not the latter, only underwent *Z-E* isomerization of the oxime without the formation of the desired products (probably due to the fast internal conversion resulting in **T2** state inactivation). For alkenyl oximes **1D** and **1F**, neither factor was satisfied, resulting in no reaction. Importantly, higher ΔE_{FO} was negatively correlated with higher ΔG_{T} (Pearson correlation coefficient of -0.75), indicating that the better matched the reaction orbitals were, the larger the ΔG_{T} was, thus the easier the reaction proceeded. Obviously, this correlation was based on the fact that the internal conversion of the **T2** state and 5-*exo-trig* cyclization in this reaction were two competing paths, the former making it easy for **T2** to decay to **T1** and the latter to convert it to the product. In this way, replacing the cumbersome ΔG^\ddagger with ΔE_{FO} can be used to establish the aforementioned criterion to rapidly assess the reactivity of substrate structures. To further confirm the accuracy of the developed criterion for structural prediction, the reactivity of a new structure of alkenyl oxime ether **1G** was predicted on this criterion (Scheme 7B). DFT evaluations showed that it was located in the first quadrant and far from the average value of ΔG_{T} and ΔE_{FO} , indicating that this structure was not suitable for the diradical epoxidation rearrangement reaction. Subsequently, we synthesized **1G** and carried out the reaction under standard reaction conditions. The desired rearrangement reaction did not occur, which fully verified the accuracy of the established criterion. During preparation of our manuscript, a related study was reported by Huang *et al.*²² Our protocol surpasses the reported one in terms of efficacy and scope, and provides new insights and an in-depth understanding of reaction mechanism and the structural requirements of the substrates through DFT calculations.

Conclusions

We developed a novel photosensitized diradical rearrangement protocol of alkenyl ketoxime ethers for synthesizing amino-featured oxiranes under the visible light-facilitated energy-transfer photocatalysis. This protocol features mild conditions, good tolerance of functional groups, wide scope of substrates, excellent diastereoselectivity and is compatible with complex scaffolds (steroids, amino acids, alkaloids). Mechanism studies revealed that the reaction initiated from excitation of the alkenyl moiety of alkenyl ketoxime ethers to triplet-state

diradical by photocatalytic energy transfer. These actions were followed by a tandem sequence of alkenyl diradical-mediated 5-*exo-trig* cyclization onto a ketoxime moiety, amino translocation, and formation of intramolecular C–O bonds. DFT calculations confirmed the proposed reaction mechanism and rationalized the excellent diastereoselectivity. A criterion for rapid assessment of reaction occurrence was also established by DFT calculations. That is, the substrate must meet both the large ΔG_{T} ($\Delta G_{\text{T}} = G_{\text{T2}[\text{alkene}]} - G_{\text{T1}[\text{oxime}]}$) and small ΔE_{FO} ($\Delta E_{\text{FO}} = E_{\text{LUMO}[\text{oxime}]} - E_{\text{HSOMO}[\text{alkene}]}$). This protocol provides a new method for the synthesis of valuable amino-featured oxiranes that were previously inaccessible, but also broadens the boundary of oxime-mediated reaction modes.

Data availability

Detailed data are in the ESI.†

Author contributions

B. H. and T. L. conceived and directed the project. T. L., L. Z., M. Q., S. L., X. W. and J. X. performed experiments. T. L., L. Z. and X. W. prepared the ESI.† B. H. wrote the paper. All authors discussed the results and commented on the manuscript.

Conflicts of interest

There are no conflicts to declare.

Acknowledgements

We thank the National Natural Science Foundation of China (22471109 and 22171118) and Science and Technology Major Program of Gansu Province of China (22ZD6FA006, 23ZDFA015, and 24ZD13FA017) for financial support.

References

- (a) D.-H. Wei, B.-L. Lei, M.-S. Tang and C.-G. Zhan, *J. Am. Chem. Soc.*, 2012, **134**, 10436–10450; (b) L.-H. Meng, R. Mohan, B. H. B. Kwok, M. Eloffsson, N. Sin and C. M. Crews, *Proc. Natl. Acad. Sci. U. S. A.*, 1999, **96**, 10403–10408; (c) J. Lee, J.-L. Liu, X.-D. Feng, M. A. S. Hernández, P. Mucka, D. Ibi, J. W. Choi and U. Ozcan, *Nat. Med.*, 2016, **22**, 1023–1032; (d) J.-S. Wang, L.-Q. Zhao, X.-W. Liu and Z.-Y. He, *Food Chem.*, 2023, **405**, 134962; (e) J. Wu, X.-Q. Wang, Y.-L. Hou and P. Gong, *Med. Chem. Res.*, 2024, **33**, 221–238; (f) Z. Y. Subeh, C. J. Pearce and N. H. Oberlies, *J. Nat. Prod.*, 2023, **86**, 596–603; (g) Y. Liu, H. Yang, Y. Liu, J. Liu, Z. Li and W. Zhang, Preparation method and application of chiral cyclopentadienyl rhodium complex, CN118580245A, 2024.
- For reviews, see: (a) J. G. Smith, *Synthesis*, 1984, **1984**, 629–656; (b) J. He, J. Ling and P. Chiu, *Chem. Rev.*, 2014, **114**, 8037–8128; (c) C. Wang, L. Luo and H. Yamamoto, *Acc. Chem. Res.*, 2016, **49**, 193–204; (d) Y. Zhang, B. Hu, Y. Chen



- and Z. Wang, *Chem.-Eur. J.*, 2024, **30**, e202402469; (e) Z. Liu, D. Wang, H. Cheng and Q. Zhou, *ChemCatChem*, 2024, **16**, e202301764; (f) A. Brandolese and A. W. Kleij, *Acc. Chem. Res.*, 2022, **55**, 1634–1645; (g) M. I. Childers, J. M. Longo, N. J. Van Zee, A. M. LaPointe and G. W. Coates, *Chem. Rev.*, 2014, **114**, 8129–8152.
- 3 For recent examples, see: (a) J. Liu, Y. Wei and P. Tang, *J. Am. Chem. Soc.*, 2018, **140**, 15194–15199; (b) A. Potrząsaj, M. Musiejuk, W. Chaładaj, M. Giedyk and D. Gryko, *J. Am. Chem. Soc.*, 2021, **143**, 9368–9376; (c) S. H. Lau, M. A. Borden, T. J. Steiman, L. S. Wang, M. Parasram and A. G. Doyle, *J. Am. Chem. Soc.*, 2021, **143**, 15873–15881; (d) Y. Wang, S. Tang, G. Yang, S. Wang, D. Ma and Y. Qiu, *Angew. Chem., Int. Ed.*, 2022, **61**, e202207746; (e) L. Li, S. Yang, Z. Xu, S. Li, J. Jiang and Y.-Q. Zhang, *J. Am. Chem. Soc.*, 2024, **146**, 13546–13557; (f) L. Li, P. Sivaguru, D. Wei, M. Liu, Q. Zhu, S. Dong, E. Casali, N. Li, G. Zanoni and X. Bi, *Nat. Commun.*, 2024, **15**, 1951; (g) W. Zhang, S. Chen, Y. Zhang, S. Liu and X. Shen, *Angew. Chem., Int. Ed.*, 2025, **64**, e202422020.
- 4 (a) Y. Usami, Y. Mizobuchi, M. Ijuin, T. Yamada, M. Morita, K. Mizuki, H. Yoneyama and S. Harusawa, *Mar. Drugs*, 2022, **20**, 438; (b) Y. Zheng, S.-H. Zhang, K. H. Low, W.-W. Zi and Z.-X. Huang, *J. Am. Chem. Soc.*, 2022, **144**, 1951–1961; (c) K. Choudhary, R. G. Biswas, A. Manna and V. K. Singh, *J. Org. Chem.*, 2023, **88**, 12041–12053.
- 5 (a) R. Goswami, *J. Am. Chem. Soc.*, 1980, **102**, 5974–5976; (b) Y. Gao, R. M. Hanson, J. M. Klunder, S. Y. Ko, H. Masamune and K. B. Sharpless, *J. Am. Chem. Soc.*, 1987, **109**, 5765–5780; (c) F. Severin, G. M. Fusì, C. Wartmann, J. M. Neudörfl and A. Berkessel, *Angew. Chem., Int. Ed.*, 2022, **61**, e202201790.
- 6 (a) E. J. Corey and M. Chaykovsky, *J. Am. Chem. Soc.*, 1962, **84**, 867; (b) E. J. Corey and M. Chaykovsky, *J. Am. Chem. Soc.*, 1965, **87**, 1353; (c) M. Szostak and J. Aubé, *J. Am. Chem. Soc.*, 2009, **131**, 13246–13247.
- 7 T. Ibuka, *Chem. Soc. Rev.*, 1998, **27**, 145–154.
- 8 A. Boucherif, Q.-Q. Yang, Q. Wang, J.-R. Chen, L.-Q. Lu and W.-J. Xiao, *J. Org. Chem.*, 2014, **79**, 3924–3929.
- 9 (a) E. Beckmann, *Ber. Dtsch. Chem. Ges.*, 1886, **19**, 988; (b) Y. Furuya, K. Ishihara and H. Yamamoto, *J. Am. Chem. Soc.*, 2005, **127**, 11240–11241; (c) X.-B. Mo, T. D. R. Morgan, H. T. Ang and D. G. Hall, *J. Am. Chem. Soc.*, 2018, **140**, 5264–5271.
- 10 (a) J. Mas-Rosello and N. Cramer, *Chem.-Eur. J.*, 2022, **28**, e202103683; (b) B. Li, J.-Z. Chen, D. Liu, I. D. Gridnev and W.-B. Zhang, *Nat. Chem.*, 2022, **14**, 920–927; (c) E. D. Heafner, A. L. Smith, C. V. Craescu, K. N. Raymond, R. G. Bergman and F. D. Toste, *Chem*, 2025, **11**, 102368.
- 11 (a) D. S. Bolotin, N. A. Bokach, M. Y. Demakova and V. Yu. Kukushkin, *Chem. Rev.*, 2017, **117**, 13039–13122; (b) R. Lavernhe, R. O. Torres-Ochoa, Q. Wang and J.-P. Zhu, *Angew. Chem., Int. Ed.*, 2021, **60**, 24028–24033.
- 12 (a) M. Kitamura and K. Narasaka, *Chem. Rec.*, 2002, **2**, 268–277; (b) H.-W. Huang, X.-C. Ji, W.-Q. Wu and H.-F. Jiang, *Chem. Soc. Rev.*, 2015, **44**, 1155–1171; (c) J. Li, Y.-T. Hu, D.-P. Zhang, Q. Liu, Y.-H. Dong and H. Liu, *Adv. Synth. Catal.*, 2017, **359**, 710–771; (d) J. Bajohr, S.-Y. Li, B. Mirabi, C. E. Johnson and M. Lautens, *Angew. Chem., Int. Ed.*, 2025, **64**, e202420479.
- 13 (a) J. Davies, S. P. Morcillo, J. J. Douglas and D. Leonori, *Chem.-Eur. J.*, 2018, **24**, 12154–12163; (b) X.-Y. Yu, Q.-Q. Zhao, J. Chen, W.-J. Xiao and J.-R. Chen, *Acc. Chem. Res.*, 2020, **53**, 1066–1083; (c) K. A. Rykaczewski, E. R. Wearing, D. E. Blackmun and C. S. Schindler, *Nat. Synth.*, 2022, **1**, 24–36; (d) X.-Y. Duan, N.-N. Zhou, R. Fang, X.-L. Yang, W. Yu and B. Han, *Angew. Chem., Int. Ed.*, 2014, **53**, 3158–3162; (e) E. M. Dauncey, S. P. Morcillo, J. J. Douglas, N. S. Sheikh and D. Leonori, *Angew. Chem., Int. Ed.*, 2018, **57**, 744–748.
- 14 (a) Q.-Q. Zhou, Y.-Q. Zou, L.-Q. Lu and W.-J. Xiao, *Angew. Chem., Int. Ed.*, 2019, **58**, 1586–1604; (b) F. Strieth-Kalthoff, M. J. James, M. Teders, L. Pitzer and F. Glorius, *Chem. Soc. Rev.*, 2018, **47**, 7190–7202; (c) S.-Y. Wen, J.-J. Chen, Y. Zheng, J.-X. Han and H.-M. Huang, *Angew. Chem., Int. Ed.*, 2025, **64**, e202415495.
- 15 (a) D. Lee, V. Soni and E. Cho, N–O Bond Activation by Energy Transfer Photocatalysis, *Acc. Chem. Res.*, 2022, **55**, 2526–2541; (b) Q. Sun, S.-P. Wang, Y. Xu, A. Yin, L. Yang, J. Zhu, C.-L. Zheng, G. Wang, Z. Fang, S. Sui, D. Wang, Y. Dong, D. Zhang, C.-S. Wang and K. Guo, *ACS Catal.*, 2025, **15**, 1854–1941.
- 16 (a) T. Patra, P. Bellotti, F. Strieth-Kalthoff and F. Glorius, *Angew. Chem., Int. Ed.*, 2020, **59**, 3172–3177; (b) T. Patra, M. Das, C. G. Daniliuc and F. Glorius, *Nat. Catal.*, 2021, **4**, 54–61; (c) G. Tan, M. Das, R. Kleinmans, F. Katzenburg, C. Daniliuc and F. Glorius, *Nat. Catal.*, 2022, **5**, 1120–1130; (d) J. E. Erchinger, R. Hoogesteger, R. Laskar, S. Dutta, C. Hümpel, D. Rana, C. G. Daniliuc and F. Glorius, *J. Am. Chem. Soc.*, 2023, **145**, 2364–2374; (e) R. Laskar, S. Dutta, J. C. Spies, P. Mukherjee, Á. Rentería-Gómez, R. E. Thielemann, C. G. Daniliuc, O. Gutierrez and F. Glorius, *J. Am. Chem. Soc.*, 2024, **146**, 10899–11090; (f) X.-X. Zhang, S.-T. Xu, X.-T. Li, T.-T. Song, D.-W. Ji and Q.-A. Chen, *J. Am. Chem. Soc.*, 2025, **147**, 11533–11542.
- 17 S.-Q. Lai, B.-Y. Wei, J.-W. Wang, W. Yu and B. Han, *Angew. Chem., Int. Ed.*, 2021, **60**, 21997–22003.
- 18 (a) M. R. Becker, A. D. Richardson and C. S. Schindler, *Nat. Commun.*, 2019, **10**, 5095–5510; (b) E. R. Wearing, Y.-C. Yeh, G. G. Terrones, S. G. Parikh, I. Kevlishvili, H. J. Kulik and C. S. Schindler, *Science*, 2024, **384**, 1468–1476.
- 19 (a) B. Han, X.-L. Yang, R. Fang, W. Yu, C. Wang, X.-Y. Duan and S. Liu, *Angew. Chem., Int. Ed.*, 2012, **51**, 8816–8820; *Angew. Chem.*, 2012, **124**, 8946–8950; (b) R.-H. Liu, D. Wei, B. Han and W. Yu, *ACS Catal.*, 2016, **6**, 6525–6530; (c) X.-X. Peng, D. Wei, W.-J. Han, F. Chen, W. Yu and B. Han, *ACS Catal.*, 2017, **7**, 7830–7834.
- 20 D. Wei, T. M. Liu, Y. H. He, B. Y. Wei, J. H. Pan, J. W. Zhang, N. Jiao and B. Han, *Angew. Chem., Int. Ed.*, 2021, **60**, 26308–26313.
- 21 Deposition number 2439472 (for **2an**) contains the supplementary crystallographic data for this paper. These data are provided free of charge by the joint Cambridge Crystallographic Data Centre and Fachinformationszentrum Karlsruhe Access Structures service.
- 22 Q.-Z. Wang, Y. Zheng, W.-T. Wu and H.-M. Huang, *J. Am. Chem. Soc.*, 2025, **147**, 16248–16254.

